

# Octupole deformation for Ba isotopes in a reflection-asymmetric relativistic mean-field approach \*

ZHANG Wei(张炜)<sup>1,2</sup> LI Zhi-Pan(李志攀)<sup>2</sup> ZHANG Shuang-Quan(张双全)<sup>2;1)</sup>

<sup>1</sup> School of Electrical Engineering and Automation, He'nan Polytechnic University, Jiaozuo 454003, China

<sup>2</sup> State Key Laboratory of Nuclear Physics and Technology, School of Physics, Peking University, Beijing 100871, China

**Abstract** The potential energy surfaces of even-even  $^{142-156}\text{Ba}$  are investigated in the constrained reflection-asymmetric relativistic mean-field approach with parameter set PK1. It is shown that for the ground states,  $^{142}\text{Ba}$  is near spherical,  $^{156}\text{Ba}$  well quadrupole-deformed, and in between  $^{144-154}\text{Ba}$  octupole deformed. In particular, the nuclei  $^{148,150}\text{Ba}$  with  $N=92, 94$  have the largest octupole deformations. By including the octupole degree of freedom, energy gaps  $N = 88, N = 94$  and  $Z = 56$  near Fermi surfaces for the single-particle levels in  $^{148}\text{Ba}$  with  $\beta_2 \sim 0.26$  and  $\beta_3 \sim 0.17$  are found. Furthermore, the performance of the octupole deformation driving pairs ( $\nu 2f_{7/2}, \nu 1i_{13/2}$ ) and ( $\pi 2d_{5/2}, \pi 1h_{11/2}$ ) is demonstrated by analyzing the single-particle levels near Fermi surfaces in  $^{148}\text{Ba}$ .

**Key words** reflection-asymmetric, relativistic mean-field, octupole deformation, single-particle levels

**PACS** 21.10.-k, 21.60.Jz, 27.60.+j

## 1 Introduction

In recent decades, the phenomena related to octupole deformation have received wide attention. Normally the regions of nuclei with strong octupole correlations correspond to either the proton or the neutron numbers close to 34 ( $1g_{9/2} \leftrightarrow 2p_{3/2}$  coupling), 56 ( $1h_{11/2} \leftrightarrow 2d_{5/2}$  coupling), 88 ( $1i_{13/2} \leftrightarrow 2f_{7/2}$  coupling) and 134 ( $1j_{15/2} \leftrightarrow 2g_{9/2}$  coupling) [1].

Extensive efforts have been made to understand the structure of neutron-rich nuclei around  $Z \sim 56$  and  $N \sim 88$ . Experimentally in this region, many octupole deformed bands have been identified and extended to higher spin, such as in  $^{139}\text{Xe}$  [2, 3], in even-even  $^{140-148}\text{Ba}$  [4–7], in  $^{144,146}\text{Ce}$  [8] and in  $^{145,147}\text{La}$  [9]. On the theoretical side, a variety of approaches have been applied to investigate the role of octupole degrees of freedom in this nuclear region. The Woods-Saxon-Bogoliubov cranking model is used to study the shapes of rotating Xe, Ba, Ce, Nd and Sm nuclei with  $N = 84 - 94$ , and the expectations of octupole-deformed mean-fields at low and medium spins are confirmed [10]. Based on the

Hartree-Fock plus BCS approximation and adiabatic time-dependent Hartree-Fock plus zero point energy in the cranking approximation, the energy splitting and  $B(E1)$  transition are well described for  $^{140}\text{Ba}$ ,  $^{142-150}\text{Ce}$ ,  $^{144-152}\text{Nd}$  and  $^{146-154}\text{Sm}$  [11]. In the *spdf* interacting boson model, good agreement of the calculated low-lying energy spectra and transition rates with data is obtained for  $^{144}\text{Ba}$  and  $^{146}\text{Ba}$  [12]. The reflection-asymmetric shell model is applied to describe the octupole deformed bands in neutron-rich  $^{142}\text{Ba}$  and  $^{145}\text{Ba}$ , and good agreement with the experimental data is obtained [13].

During recent years, the Relativistic Mean-Field (RMF) theory [14–16] has achieved great success in describing many nuclear phenomena related to stable nuclei [14] and exotic nuclei [17, 18], as well as supernova and neutron stars [19]. Recently, the Reflection-ASymmetric Relativistic Mean-Field (RAS-RMF) approach considering the octupole degrees of freedom has been developed and applied to the well-known octupole deformed nucleus  $^{226}\text{Ra}$  [20], and La isotopes [21]. In Ref. [22], the RAS-RMF approach has been applied to investigate the potential

Received 1 March 2010

\* Supported by Foundation of He'nan Educational Committee (200614003), Young Backbone Teacher Support Program of He'nan Polytechnic University, China Postdoctoral Science Foundation, Major State Basic Research Developing Program (2007CB815000) and National Natural Science Foundation of China (10775004, 10975007, 10975008)

1) E-mail: sqzhang@pku.edu.cn

©2010 Chinese Physical Society and the Institute of High Energy Physics of the Chinese Academy of Sciences and the Institute of Modern Physics of the Chinese Academy of Sciences and IOP Publishing Ltd

energy surfaces (PESs) of even-even  $^{146-156}\text{Sm}$  isotopes in the  $(\beta_2, \beta_3)$  plane. It is suggested that the critical-point candidate nucleus  $^{152}\text{Sm}$  marks the shape/phase transition not only from  $U(5)$  to  $SU(3)$  symmetry, but also from the octupole deformed ground state in  $^{150}\text{Sm}$  to quadrupole deformed ground state in  $^{154}\text{Sm}$ . Therefore, it is interesting to investigate the Ba isotopes in the RAS-RMF approach.

In this paper, the RAS-RMF approach will be applied to investigate the potential energy surfaces of even-even  $^{142-156}\text{Ba}$  isotopes in the  $(\beta_2, \beta_3)$  plane, and the single-particle levels near Fermi surfaces for the nucleus  $^{148}\text{Ba}$  will be studied.

## 2 Formalism

The basic ansatz of the RMF theory is a Lagrangian density where nucleons are described as Dirac particles that interact via the exchange of various mesons and the photon. The mesons considered are the isoscalar-scalar  $\sigma$ , the isoscalar-vector  $\omega$  and the isovector-vector  $\rho$ . The effective Lagrangian density reads [23]

$$\begin{aligned} \mathcal{L} = & \bar{\psi} \left[ i\gamma^\mu \partial_\mu - M - g_\sigma \sigma - g_\omega \gamma^\mu \omega_\mu - \right. \\ & \left. g_\rho \gamma^\mu \vec{\tau} \cdot \vec{\rho}_\mu - e\gamma^\mu \frac{1-\tau_3}{2} A_\mu \right] \psi + \\ & \frac{1}{2} \partial^\mu \sigma \partial_\mu \sigma - \frac{1}{2} m_\sigma^2 \sigma^2 - \frac{1}{3} g_2 \sigma^3 - \frac{1}{4} g_3 \sigma^4 - \\ & \frac{1}{4} \Omega^{\mu\nu} \Omega_{\mu\nu} + \frac{1}{2} m_\omega^2 \omega^\mu \omega_\mu + \frac{1}{4} c_3 (\omega^\mu \omega_\mu)^2 - \\ & \frac{1}{4} \vec{R}^{\mu\nu} \cdot \vec{R}_{\mu\nu} + \frac{1}{2} m_\rho^2 \vec{\rho}^\mu \cdot \vec{\rho}_\mu - \frac{1}{4} F^{\mu\nu} F_{\mu\nu}, \end{aligned} \quad (1)$$

in which the field tensors for the vector mesons and the photon are respectively defined as

$$\begin{cases} \Omega_{\mu\nu} = \partial_\mu \omega_\nu - \partial_\nu \omega_\mu, \\ \vec{R}_{\mu\nu} = \partial_\mu \vec{\rho}_\nu - \partial_\nu \vec{\rho}_\mu, \\ F_{\mu\nu} = \partial_\mu A_\nu - \partial_\nu A_\mu. \end{cases} \quad (2)$$

Using the classical variational principle, one can obtain the Dirac equation for the nucleons and the Klein-Gordon equations for the mesons. To solve these equations, we employ the basis expansion method, which has been widely used in both the non-relativistic and the relativistic mean-field models. For axial-symmetric reflection-asymmetric systems, the spinors are expanded in terms of the eigenfunctions of the Two-Center Harmonic-Oscillator (TCHO) po-

tential:

$$V(r_\perp, z) = \frac{1}{2} M \omega_\perp^2 r_\perp^2 + \begin{cases} \frac{1}{2} M \omega_1^2 (z + z_1)^2, & z < 0, \\ \frac{1}{2} M \omega_2^2 (z - z_2)^2, & z \geq 0, \end{cases} \quad (3)$$

where  $M$  is the nucleon mass,  $z_1$  and  $z_2$  (real, positive) represent the distances between the centers of the spheroids and their intersection plane, and  $\omega_1$  ( $\omega_2$ ) are the corresponding oscillator frequencies for  $z < 0$  ( $z \geq 0$ ) [20]. The TCHO basis has been widely used in the studies of fission, fusion, heavy-ion emission and various cluster phenomena [24]. By setting proper asymmetric parameters, the major and  $z$ -axis quantum numbers are real numbers very close to integers, and the integers are used in the Nilsson-like notation  $\Omega[Nn_z m_l]$  for convenience. More details can be found in Ref. [20].

The binding energy at a certain deformation is obtained by constraining the mass quadrupole moment  $\langle \hat{Q}_2 \rangle$  to a given value  $\mu_2$  [25], i.e.,

$$\langle H' \rangle = \langle H \rangle + \frac{1}{2} C (\langle \hat{Q}_2 \rangle - \mu_2)^2, \quad (4)$$

where  $C$  is the curvature constant parameter and  $\mu_2$  is the given quadrupole moment. The expectation value of  $\hat{Q}_2$  is  $\langle \hat{Q}_2 \rangle = \langle \hat{Q}_2 \rangle_n + \langle \hat{Q}_2 \rangle_p$  with  $\langle \hat{Q}_2 \rangle_{n,p} = \langle 2r^2 P_2(\cos\theta) \rangle_{n,p}$ . The deformation parameter  $\beta_2$  is related to  $\langle \hat{Q}_2 \rangle$  by  $\langle \hat{Q}_2 \rangle = \frac{3}{\sqrt{5}\pi} A r^2 \beta_2$ , with  $r = R_0 A^{1/3}$  ( $R_0 = 1.2$  fm) and  $A$  the mass number. The octupole moment constraint can also be applied similarly with  $\langle \hat{Q}_3 \rangle = \langle \hat{Q}_3 \rangle_n + \langle \hat{Q}_3 \rangle_p$ ,  $\langle \hat{Q}_3 \rangle_{n,p} = \langle 2r^3 P_3(\cos\theta) \rangle_{n,p}$  and  $\langle \hat{Q}_3 \rangle = \frac{3}{\sqrt{7}\pi} A r^3 \beta_3$ . By constraining the quadrupole moment and octupole moment simultaneously, the total energy surface in  $(\beta_2, \beta_3)$  plane can be obtained.

## 3 Results and discussion

The properties of even-even  $^{142-156}\text{Ba}$  are calculated in the constrained RAS-RMF approach with parameter set PK1 [26]. The TCHO basis with 16 major shells for both fermions and bosons is used. The pairing correlation is treated by the BCS approximation with a constant pairing gap  $\Delta = 11.2/\sqrt{A}$  MeV.

To investigate the shape evolution in  $^{142-156}\text{Ba}$ , the total energies as functions of  $\beta_2$  and  $\beta_3$  have been analyzed. As an example, Fig. 1 displays the contour plots for  $^{142}\text{Ba}$  and  $^{148}\text{Ba}$ . It is found that, for the ground states,  $^{142}\text{Ba}$  is near spherical without octupole deformation,  $^{144-154}\text{Ba}$  octupole deformed and  $^{156}\text{Ba}$  well quadrupole-deformed. In detail, for  $^{144-156}\text{Ba}$ , the quadrupole deformation  $\beta_2$  of the global

octupole minimum gradually increases with increasing neutron numbers. On the other hand, the octupole deformation  $\beta_3$  of the global octupole minimum gradually increases for  $^{144,146,148}\text{Ba}$ , and decreases for  $^{150,152,154}\text{Ba}$ , and until  $^{156}\text{Ba}$  the global minimum is well deformed with little octupole de-

formation. A soft area covering the global octupole minimum and the saddle point at  $\beta_3=0$  appears in  $^{144}\text{Ba}$ , and develops in  $^{146-154}\text{Ba}$ . Furthermore, the energy difference between the global octupole minimum and the saddle point increases from  $^{144}\text{Ba}$  to  $^{148}\text{Ba}$ , while it decreases from  $^{150}\text{Ba}$  to  $^{156}\text{Ba}$ .

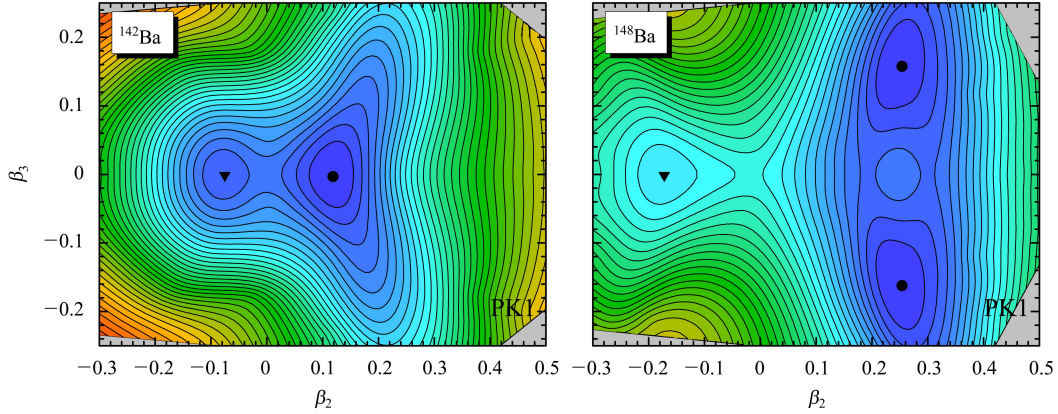


Fig. 1. (Color online) The contour plots of total energies for even-even  $^{142}\text{Ba}$  and  $^{148}\text{Ba}$  in  $(\beta_2, \beta_3)$  plane obtained in RAS-RMF approach with PK1 and constant- $\Delta$  pairing. The energy separation between contour lines is 0.5 MeV. The global minimum and other local minima are denoted by “•” and “▼”, respectively.

The binding energy, quadrupole and octupole deformations are summarized for the ground states of even-even  $^{142-156}\text{Ba}$  in Table 1. The binding energies are well reproduced within 0.3%. Moreover, excellent agreement is obtained for the quadrupole deformations. It's indicated that the ground states of even-even  $^{144-154}\text{Ba}$  with  $N = 88 - 98$  are octupole deformed, while in the middle the nuclei  $^{148,150}\text{Ba}$  with  $N = 92 - 94$  are the most octupole deformed. It is noted that the suggested octupole Ba nuclei ( $N = 88 - 98$ ) are more neutron-rich than those ( $N = 86 - 91$ ) predicted in the finite-range droplet

Table 1. The total binding energy (in MeV) as well as the quadrupole deformation  $\beta_2$  and octupole deformation  $\beta_3$  of the ground states of even-even  $^{142-156}\text{Ba}$  obtained in the constrained RAS-RMF approach with PK1, in comparison with the available experimental data.

nucleus	$E^{\text{cal}}$	$\beta_2^{\text{cal}}$	$\beta_3^{\text{cal}}$	$E^{\text{exp}}$ [27]	$\beta_2^{\text{exp}}$ [28]
$^{142}\text{Ba}$	1181.25	0.12	0.00	1180.14	0.16
$^{144}\text{Ba}$	1190.19	0.20	0.12	1190.23	0.19
$^{146}\text{Ba}$	1199.06	0.23	0.13	1199.60	0.22
$^{148}\text{Ba}$	1207.26	0.26	0.17	1208.76	—
$^{150}\text{Ba}$	1215.12	0.28	0.17	1217.55	—
$^{152}\text{Ba}$	1221.86	0.30	0.12	1225.58	—
$^{154}\text{Ba}$	1228.30	0.32	0.08	—	—
$^{156}\text{Ba}$	1234.58	0.33	0.03	—	—

model [29]. This conclusion consists with the previous RAS-RMF calculation for La isotopes [21].

To understand the evolution of the octupole deformation, the microscopic single-particle levels are analyzed. Fig. 2 shows the neutron single-particle levels for the states minimized with respect to  $\beta_3$  and the states with  $\beta_3=0$  for  $\beta_2 = 0.14-0.38$  in  $^{148}\text{Ba}$  side by side. The levels near the Fermi surface are labeled by Nilsson-like notations  $\Omega[Nn_z m_l]$  of the largest component. In the left panel of Fig. 2, an energy gap  $N = 88$  fenced with several levels near the Fermi surface for  $\beta_2 = 0.20-0.30$  is found approaching the octupole minimum. Additionally, a gap at  $N = 94$  is found for  $\beta_2 \sim 0.28$ . For the states with  $\beta_3=0$ , the neutron gap at  $N = 88$  is relatively small, and the gap at  $N = 94$  does not appear. Furthermore, the proton single-particle levels for the corresponding states are shown in Fig. 3. An energy gap  $Z = 56$  appears for the states with octupole deformation approaching the ground state in the left panel of Fig. 3, while the energy gap  $Z = 56$  cannot be found near the Fermi surfaces for the states with  $\beta_3=0$  in the right panel of Fig. 3. Thus the energy gaps  $N = 88$ ,  $N = 94$  and  $Z = 56$  near Fermi surfaces are responsible for the octupole minimum of Ba isotopes. In particular, the energy gaps  $N = 94$  and  $Z = 56$  around  $\beta_2 \sim 0.28$  are consistent with the large octupole deformation predicted for  $^{148,150}\text{Ba}$ .

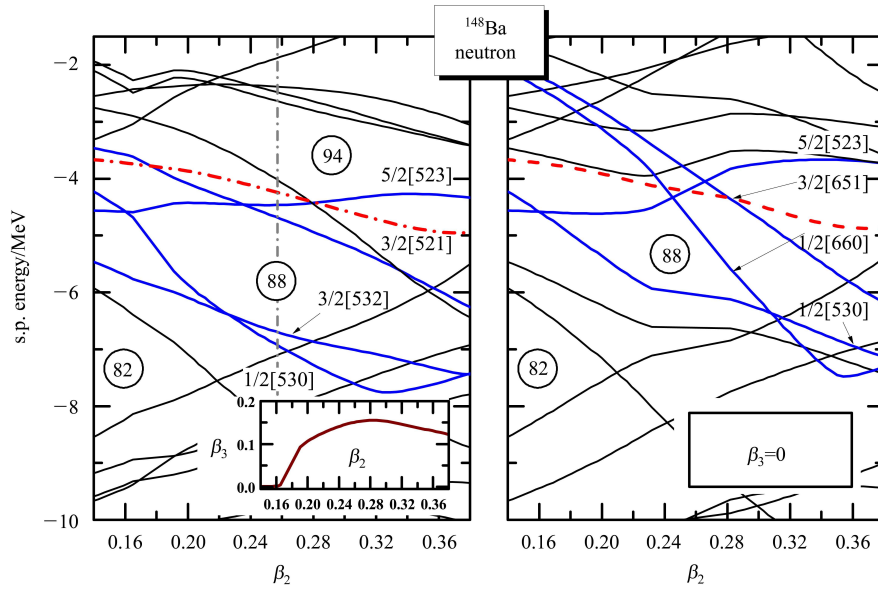


Fig. 2. (Color online) Neutron single-particle levels of  $^{148}\text{Ba}$  in RAS-RMF approach with PK1 as functions of  $\beta_2$  for states minimized with respect to  $\beta_3$  (left panel) and states with  $\beta_3=0$  (right panel). The dash-dot lines denote the corresponding Fermi surfaces. The levels near the Fermi surface are labeled by Nilsson-like notations  $\Omega[Nn_z m_i]$  of the first component. The corresponding  $\beta_3$  are shown in the inset. The quadrupole deformation of the ground state is indicated by the vertical gray line.

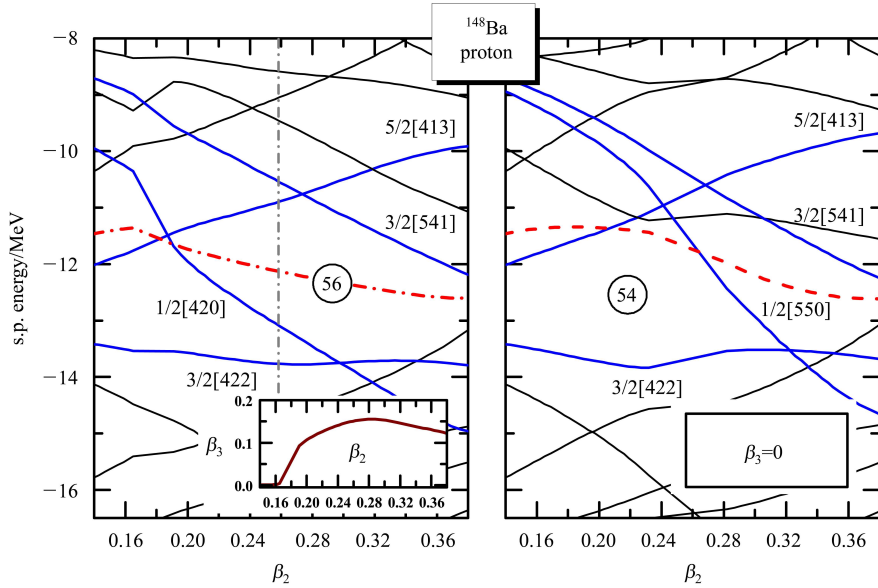


Fig. 3. (Color online) Same as Fig. 2, but for the proton.

It is well known that, for nuclei with  $N \sim 88$  or  $Z \sim 56$ , the octupole deformation driving pairs of orbitals include  $(\nu 2f_{7/2}, \nu 1i_{13/2})$  and  $(\pi 2d_{5/2}, \pi 1h_{11/2})$ , which in the axially deformed case will be subgrouped as  $(\nu 1/2[541], \nu 1/2[660])$ ,  $(\nu 3/2[532], \nu 3/2[651])$ ,  $(\nu 5/2[523], \nu 5/2[642])$ ,  $(\nu 7/2[514], \nu 7/2[633])$ , and  $(\pi 1/2[431], \pi 1/2[550])$ ,  $(\pi 3/2[422], \pi 3/2[541])$ ,  $(\pi 5/2[413], \pi 5/2[532])$ , respectively. It

is interesting to investigate the performance of such pairs in the single-particle levels near Fermi surfaces in Figs. 2 and 3. These levels, together with their BCS occupation probabilities and their ten leading components for the ground state, are shown in Tables 2 and 3, respectively. Taking the level  $\nu 3/2[521]$  as an example, its second (18.7%) and third (16.5%) components comprise an octupole deformation driv-

ing pair ( $\nu 3/2[532]$ ,  $\nu 3/2[651]$ ). Similarly, one can find the pair ( $1/2[541]$ ,  $1/2[660]$ ) for  $\nu 1/2[530]$ , the pair ( $3/2[532]$ ,  $3/2[651]$ ) for  $\nu 3/2[532]$  and the pair ( $5/2[523]$ ,  $5/2[642]$ ) for  $\nu 5/2[523]$ . For the proton side, octupole deformation driving pairs are also

found among the components of single-particle levels near Fermi surfaces at the ground state of  $^{148}\text{Ba}$ . Therefore, both the neutron and the proton driving pairs play important roles for the octupole minimum in  $^{148}\text{Ba}$ .

Table 2. Single-particle levels near Fermi surface for the ground state in  $^{148}\text{Ba}$ , together with their BCS occupation probabilities and corresponding contributions from the ten leading components. The components originating from the octupole deformation driving pairs of orbitals ( $\nu 2f_{7/2}$ ,  $\nu 1i_{13/2}$ ) and ( $\pi 2d_{5/2}$ ,  $\pi 1h_{11/2}$ ) are in bold. This table is for the neutron.

level	$\nu 1/2[530]$		$\nu 3/2[532]$		$\nu 3/2[521]$		$\nu 5/2[523]$	
occu.	0.973		0.968		0.721		0.609	
1st comp.	1/2[530]	41.0%	<b>3/2[532]</b>	<b>52.6%</b>	3/2[521]	36.0%	<b>5/2[523]</b>	<b>56.4%</b>
2nd comp.	<b>1/2[541]</b>	<b>15.6%</b>	3/2[541]	17.6%	<b>3/2[532]</b>	<b>18.7%</b>	5/2[532]	12.7%
3rd comp.	<b>1/2[660]</b>	<b>6.2%</b>	3/2[512]	6.2%	<b>3/2[651]</b>	<b>16.5%</b>	<b>5/2[642]</b>	<b>10.1%</b>
4th comp.	1/2[651]	5.8%	<b>3/2[651]</b>	<b>6.0%</b>	3/2[631]	6.8%	5/2[633]	5.0%
5th comp.	1/2[510]	5.7%	3/2[631]	3.7%	3/2[642]	6.7%	5/2[622]	3.3%
6th comp.	1/2[631]	3.5%	3/2[521]	2.2%	3/2[761]	2.5%	5/2[503]	3.2%
7th comp.	1/2[640]	3.2%	3/2[761]	1.7%	3/2[501]	2.1%	5/2[512]	2.0%
8th comp.	1/2[770]	3.1%	3/2[402]	1.6%	3/2[622]	2.0%	5/2[413]	1.3%
9th comp.	1/2[400]	2.6%	3/2[642]	1.1%	3/2[721]	0.9%	5/2[752]	0.8%
10th comp.	1/2[521]	1.9%	3/2[321]	0.9%	3/2[752]	0.8%	5/2[613]	0.5%

Table 3. Same as Table 2, but for the proton.

level	$\pi 3/2[422]$		$\pi 1/2[420]$		$\pi 5/2[413]$		$\pi 3/2[541]$	
occu.	0.936		0.863		0.098		0.068	
1st comp.	<b>3/2[422]</b>	<b>69.4%</b>	1/2[420]	38.6%	<b>5/2[413]</b>	<b>78.7%</b>	<b>3/2[541]</b>	<b>40.8%</b>
2nd comp.	3/2[431]	10.7%	<b>1/2[550]</b>	<b>14.4%</b>	5/2[422]	8.9%	3/2[521]	15.3%
3rd comp.	3/2[402]	5.1%	1/2[530]	11.0%	5/2[523]	4.2%	3/2[411]	13.9%
4th comp.	<b>3/2[541]</b>	<b>3.8%</b>	1/2[541]	8.6%	<b>5/2[532]</b>	<b>2.0%</b>	3/2[532]	10.2%
5th comp.	3/2[532]	2.0%	1/2[400]	4.2%	5/2[303]	1.7%	<b>3/2[422]</b>	<b>7.1%</b>
6th comp.	3/2[521]	1.7%	1/2[521]	3.7%	5/2[512]	0.5%	3/2[651]	2.2%
7th comp.	3/2[312]	1.4%	1/2[660]	3.3%	5/2[813]	0.1%	3/2[512]	1.9%
8th comp.	3/2[211]	0.7%	<b>1/2[431]</b>	<b>2.7%</b>	5/2[633]	0.1%	3/2[431]	1.1%
9th comp.	3/2[651]	0.5%	1/2[220]	1.6%	5/2[833]	0.1%	3/2[761]	0.9%
10th comp.	3/2[642]	0.3%	1/2[411]	1.5%	5/2[312]	0.1%	3/2[321]	0.6%

## 4 Summary

In conclusion, the PESs of even-even  $^{142-156}\text{Ba}$  in ( $\beta_2$ ,  $\beta_3$ ) plane are investigated by the constrained RAS-RMF approach, and the single-particle levels near Fermi surfaces for the nucleus  $^{148}\text{Ba}$  are studied. It is shown that, for the ground states,  $^{142}\text{Ba}$  is near spherical without octupole deformation,  $^{144-154}\text{Ba}$  octupole deformed and  $^{156}\text{Ba}$  well quadrupole-deformed. The nuclei with largest octupole deformation  $\beta_3$  for the ground states are predicted to be  $^{148,150}\text{Ba}$  ( $N = 92, 94$ ).

By including the octupole degree of freedom, energy gaps  $N = 88$ ,  $N = 94$  and  $Z = 56$  near Fermi surfaces are found in single-particle levels approaching the ground state of  $^{148}\text{Ba}$ . Furthermore, the performance of the octupole deformation driving pairs ( $\nu 2f_{7/2}$ ,  $\nu 1i_{13/2}$ ) and ( $\pi 2d_{5/2}$ ,  $\pi 1h_{11/2}$ ) is demonstrated by analyzing the components of the single-particle levels near Fermi surfaces.

*The authors gratefully acknowledge Professor MENG Jie, Dr. GENG Li-Sheng and LIANG Hao-Zhao for their helpful suggestions and stimulating discussions.*

## References

- 1 Butler P A, Nazarewicz W. *Rev. Mod. Phys.*, 1996, **68**: 349
- 2 ZHU S J, Hamilton J H, Ramayya A V et al. *J. Phys. G*, 1997, **23**: L77
- 3 LUO Y X, Rasmussen J O, Hamilton J H et al. *Phys. Rev. C*, 2002, **66**: 014305
- 4 Phillips W R, Ahmad I, Emling H et al. *Phys. Rev. Lett.*, 1986, **57**: 3257
- 5 ZHU S J, LU Q H, Hamilton J H et al. *Phys. Lett.*, 1995, **B357**: 273
- 6 ZHU S J, WANG M G, Hamilton J H et al. *Chin. Phys. Lett.*, 1997, **14**(8): 569
- 7 Urban W, Jones M A, Durell J L et al. *Nucl. Phys.*, 1997, **A613**: 107
- 8 ZHU L Y, ZHU S J, LI M et al. *HEP & NP*, 1998, **22**: 885 (in Chinese)
- 9 ZHU S J, Hamilton J H, Ramayya A V et al. *Phys. Rev. C*, 1999, **59**: 1316
- 10 Nazarewicz W, Tabor S L. *Phys. Rev. C*, 1992, **45**: 2226
- 11 Egido J L, Robledo L M. *Nucl. Phys.*, 1992, **A545**: 589
- 12 LIU Y X, SUN H Z, ZHAO E G. *J. Phys. G*, 1994, **20**: 1771
- 13 CHEN Y J, CHEN Y S, ZHU S J et al. *Chin. Phys. Lett.*, 2005, **22**: 1362
- 14 Ring P. *Prog. Part. Nucl. Phys.*, 1996, **37**: 193
- 15 Vretenar D, Afanasiev A V, Lalazissis G A et al. *Phys. Rep.*, 2005, **409**: 101
- 16 MENG J, Toki H, ZHOU S G et al. *Prog. Part. Nucl. Phys.*, 2006, **57**: 470
- 17 MENG J, Ring P. *Phys. Rev. Lett.*, 1996, **77**: 3963
- 18 MENG J, Ring P. *Phys. Rev. Lett.*, 1998, **80**: 460
- 19 Glendenning N K. *Compact Stars*. New York: Springer-Verlag, 2000. 1
- 20 GENG L S, MENG J, Toki H. *Chin. Phys. Lett.*, 2007, **24**: 1865
- 21 WANG N, GUO L. *Sci. China Ser. G*, 2009, **52**(10): 1574
- 22 ZHANG W, LI Z P, ZHANG S Q, MENG J. *Phys. Rev. C*, 2010, **81**: 034302
- 23 Serot B D, Walecka J D. *Adv. Nucl. Phys.*, 1986, **16**: 1
- 24 Greiner W, Park J Y, Scheid W. *Nuclear Molecules*. Singapore: World Scientific, 1994. 1
- 25 Ring P, Schuck P. *The Nuclear Many-body Problem*. New York: Springer-Verlag, 1980. 1
- 26 LONG W H, MENG J, Giai N V et al. *Phys. Rev. C*, 2004, **69**: 034319
- 27 Audi G, Wapstra A H, Thibault C, *Nucl. Phys.*, 2003, **A729**: 337
- 28 Raman S, Nestor Jr. C W, Tikkanen P. *At. Data Nucl. Data Tables*, 2001, **78**: 1
- 29 Möller P, Nix J R, Myers W D et al. *At. Data Nucl. Data Tables*, 1995, **59**: 185